REPORT DOCUMENTATION PAGE

Form Approved OMB NO. 0704-0188

The public reporting burden for this collection of information is estimated to average 1 hour per response, including the time for reviewing instructions, searching existing data sources, gathering and maintaining the data needed, and completing and reviewing the collection of information. Send comments regarding this burden estimate or any other aspect of this collection of information, including suggesstions for reducing this burden, to Washington Headquarters Services, Directorate for Information Operations and Reports, 1215 Jefferson Davis Highway, Suite 1204, Arlington VA, 22202-4302. Respondents should be aware that notwithstanding any other provision of law, no person shall be subject to any oenalty for failing to comply with a collection of information if it does not display a currently valid OMB control number.
PLEASE DO NOT RETURN YOUR FORM TO THE ABOVE ADDRESS.

1. REPORT DATE (DD-MM-YYYY)	2. REPORT TYPE	3. DATES COVERED (From - To)
31-08-2021	Final Report	1-May-2017 - 31-May-2021

4. TITLE AND SUBTITLE
Final Report: Mechanisms of Force and Moment Generation by the Flow Over Oscillating Rectangular Cylinders

5a. CONTRACT NUMBER
W911NF-17-1-0153

5b. GRANT NUMBER

5c. PROGRAM ELEMENT NUMBER
611102

6. AUTHORS

5d. PROJECT NUMBER

5e. TASK NUMBER

5f. WORK UNIT NUMBER

7. PERFORMING ORGANIZATION NAMES AND ADDRESSES
Michigan State University
Hannah Administration Building
426 Auditorium Road, Room 2
East Lansing, MI 48824 -2600

8. PERFORMING ORGANIZATION REPORT NUMBER

9. SPONSORING/MONITORING AGENCY NAME(S) AND ADDRESS (ES)
U.S. Army Research Office
P.O. Box 12211
Research Triangle Park, NC 27709-2211

10. SPONSOR/MONITOR'S ACRONYM(S)
ARO

11. SPONSOR/MONITOR'S REPORT NUMBER(S)
69817-EG.8

12. DISTRIBUTION AVAILIBILITY STATEMENT
Approved for public release; distribution is unlimited.

13. SUPPLEMENTARY NOTES
The views, opinions and/or findings contained in this report are those of the author(s) and should not contrued as an official Department of the Army position, policy or decision, unless so designated by other documentation.

14. ABSTRACT

15. SUBJECT TERMS

16. SECURITY CLASSIFICATION OF:			17. LIMITATION OF ABSTRACT	15. NUMBER OF PAGES	19a. NAME OF RESPONSIBLE PERSON
a. REPORT	b. ABSTRACT	c. THIS PAGE			Ahmed Naguib
UU	UU	UU	UU		19b. TELEPHONE NUMBER 517-432-1616

RPPR Final Report
as of 18-Oct-2021

Agency Code: 21XD

Proposal Number: 69817EG **Agreement Number: W911NF-17-1-0153**
INVESTIGATOR(S):

Name: Ahmed Naguib
Email: NAGUIB@EGR.MSU.EDU
Phone Number: 5174321616
Principal: Y

Organization: **Michigan State University**
Address: Hannah Administration Building, East Lansing, MI 488242600
Country: USA

DUNS Number: 193247145 EIN: 386005984
Report Date: 31-Aug-2021 Date Received: 31-Aug-2021
Final Report for Period Beginning 01-May-2017 and Ending 31-May-2021
Title: Mechanisms of Force and Moment Generation by the Flow Over Oscillating Rectangular Cylinders
Begin Performance Period: 01-May-2017 **End Performance Period:** 31-May-2021
Report Term: 0-Other

Submitted By: Ahmed Naguib Email: NAGUIB@EGR.MSU.EDU
Phone: (517) 432-1616

Distribution Statement: 1-Approved for public release; distribution is unlimited.

STEM Degrees: 1 **STEM Participants:**

Major Goals: The key goals of this project may be summarized as follows:

1) To establish the galloping instability characteristics of sharp-corner rectangular cross-section cylinders with different side ratios (i.e. chord to thickness ratios c/d) in the range 1?c/d?3, and Reynolds number 1,000-10,000, using measurements of the aerodynamic load on the cylinder at different angles of attack ?;

2) To investigate the effect of the rectangle's corner radius (r/d) and surface topology on galloping instability characteristics of the cylinders;

3) To identify cases of interest based on the outcome of parts 1 and 2, and study the aerodynamics load of these cases under dynamic (forced-oscillation) conditions;

4) To connect the observed aerodynamic load behavior, and galloping instability characteristics, under static and dynamic conditions to the underlying flow physics. This will be accomplished using Molecular Tagging Velocimetry measurements of the boundary layer resolved velocity profiles along the model's surface and the cross-stream profiles in the wake.

Accomplishments: The following list provides a summary of the main accomplishments during the entirety of the project. Technical details of items 1 through 3 on the list have been published in three journal and four conference papers. Interested readers may consult these publications for details of the work. For items 4 and 5 on the list, further details are given in section IV of the attached technical report. Also, references cited below can be found in the attached technical report.

1) A new experimental setup and procedure were established to study galloping instability characteristics of rectangular cylinders having different geometrical parameters at low Reynolds number (1,000 < Re < 10,000) in a wind tunnel. This effort specifically includes:

* Developing a new one-component high-sensitivity mean-force balance to enable measurement of the very low magnitude force encountered in the target Reynold number range. Details of the force balance is published in [4];

* Fabricating cylinder models with provisions to enable measurement of the surface pressure distribution around the model (in addition to force measurements) [5] and [6];

* Establishing a procedure for systematically defining, fabricating and characterizing cylinder models having surface topology [7] and [8].

2) A static-force measurement campaign was completed in the wind tunnel to characterize the plunge galloping instability for rectangular cylinders with various geometrical features, including corner radius, side ratio and surface topology. The bulk of the force measurement results have been published in [5-8];

3) A measurement campaign was completed in a 15 cm×15 cm water tunnel to examine the effect of surface topology on the boundary layer and the wake flow of rectangular cylinders. The experiments, which utilized one-component Molecular Tagging Velocimetry (1c-MTV), were undertaken in order to understand the flow physics leading to the observed force characteristics documented in the wind tunnel experiments described in item 2 above. The main findings from the MTV measurements are published in AIAA SciTech 2020 and 2021 conference proceedings [9] and [10]. Additional findings are the subject of an AIAA SciTech 2022 abstract that is currently under review;

4) A set of experiments was completed in a larger 60 cm×60 cm water tunnel to study the unsteady force characteristics of harmonically heaving rectangular cylinders. The geometry of the models examined was selected based on the outcome of the study described in item 2 above. Key findings from this part of the study are summarized in section IV.A in the attached technical report;

5) 1c-MTV experiments complementing the force measurements in item 4 were carried out on the heaving cylinders. Results from these experiments uncovered non-quasi-steady behavior of the separated shear layer, leading to hypotheses regarding the connection between this behavior and galloping instability of the cylinders. Highlights of the findings from the 1c-MTV experiments can be found in section IV.B in the attached technical report.

Training Opportunities: Two postdoctoral researchers and one graduate student carried out the research work of this project. The postdoctoral researchers are Mark Feero and Alireza Safaripour. Upon completion of his two-year postdoc between September 1st, 2017 - August 31st, 2019, Feero assumed a position with RWDI in Toronto, Canada, where he is responsible for planning and executing wind-tunnel experiments related to wind-structure interaction to guide the design of bridges, buildings, etc. Safaripour worked on this project between February 1st, 2020 - May 31st, 2021. He has just started a position with University of Texas Dallas, to manage their large (2.8m x 2.1m x 30m) Boundary Layer and Subsonic Wind Tunnel (BLAST), which is used for various research aspects with a good deal of focus on wind turbines. The graduate student, Kian Kalan, completed a Master's degree in Mechanical Engineering working on this project. He continues to work on research related to this project for his PhD thesis work. He is expected to complete his PhD work in 2022.

Results Dissemination: Parts of the main findings of this project have been published in three journal and four conference papers. These papers are cited in the attached technical report and are uploaded in Products section. Additionally, a total of eight conference presentations were given on research results emerging from this project. Four of these presentations are connected with the conference paper mentioned above, and the other four were given at the American Physical Society (APS), Division of Fluid Dynamics annual meetings between 2018 and 2020. There are no papers associated with this meeting; only short abstracts. There is also one extended abstract under review for the American Institute of Aeronautics and Astronautics (AIAA) SciTech 2022 conference next January, and we expect an additional 2-3 journal publications on data that have been acquired but not fully analyzed yet.

Honors and Awards: Ahmed Naguib received a Fulbright Scholar award in the spring of 2021 that will fund sabbatical work at University of Rostock in Rostock, Germany in the period January 1st - May 31st, 2022. The Fulbright program is sponsored by the U.S. Department of State’s Bureau of Educational and Cultural Affairs.

Manoochehr Koochesfahani received the University Distinguished Professor designation at Michigan State University in the spring of 2021. UDP designation is the highest honor given by MSU to faculty that are recognized for their exceptional scholarship and service.

Protocol Activity Status:

Technology Transfer: Nothing to Report

RPPR Final Report
as of 18-Oct-2021

PARTICIPANTS:

Participant Type: PD/PI
Participant: Ahmed M Naguib
Person Months Worked: 1.00 **Funding Support:**
Project Contribution:
National Academy Member: N

Participant Type: Co PD/PI
Participant: Manoochehr M Koochesfahani
Person Months Worked: 1.00 **Funding Support:**
Project Contribution:
National Academy Member: N

Participant Type: Graduate Student (research assistant)
Participant: Kian Kalan
Person Months Worked: 12.00 **Funding Support:**
Project Contribution:
National Academy Member: N

Participant Type: Postdoctoral (scholar, fellow or other postdoctoral position)
Participant: Mark Feero
Person Months Worked: 12.00 **Funding Support:**
Project Contribution:
National Academy Member: N

Participant Type: Postdoctoral (scholar, fellow or other postdoctoral position)
Participant: Alireza Safaripour
Person Months Worked: 15.00 **Funding Support:**
Project Contribution:
National Academy Member: N

ARTICLES:

RPPR Final Report
as of 18-Oct-2021

Publication Type: Journal Article Peer Reviewed: Y **Publication Status:** 1-Published
Journal: Measurement Science and Technology
Publication Identifier Type: DOI Publication Identifier: 10.1088/1361-6501/ab2dd6
Volume: Issue: First Page #:
Date Submitted: 8/27/19 12:00AM Date Published: 6/1/19 8:00AM
Publication Location:
Article Title: Single-component force balance for the measurement of low-magnitude mean aerodynamic loads
Authors: Mark Feero, Ahmed Naguib, Manoochehr M Koochesfahani
Keywords: Sensor development, aerodynamic force measurements
Abstract: A novel force balance is developed for the measurement of low-magnitude mean aerodynamic forces. The measurement of such small loads is often desired for low Reynolds number wind tunnel experiments, however, commercially available options for force measurement do not have high enough sensitivity or accuracy. A force balance is designed to measure forces that range from O(1) mN to hundreds of milli-Newtons in magnitude. The sensitivity of the balance is derived theoretically, and the actual value is determined from calibration. The force balance demonstrates both a high degree of linearity, and low hysteresis over the desired load range. The measurement capability of the force balance is validated using measurements of the drag force on a circular cylinder, and the lift force on a square cylinder for Reynolds numbers between 1100 and 10,000.
Distribution Statement: 3-Distribution authorized to U.S. Government Agencies and their contractors
Acknowledged Federal Support: **Y**

Publication Type: Journal Article Peer Reviewed: Y **Publication Status:** 1-Published
Journal: Journal of Fluids and Structures
Publication Identifier Type: DOI Publication Identifier: 10.1016/j.jfluidstructs.2020.102881
Volume: 94 Issue: First Page #: 102881
Date Submitted: 8/29/20 12:00AM Date Published: 4/1/20 4:00AM
Publication Location:
Article Title: Influence of geometry on the galloping instability of rectangular cylinders in the Reynolds number range 1,000–10,000
Authors: Mark A. Feero, Ahmed M. Naguib, Manoochehr M. Koochesfahani
Keywords: Flow-Induce Vibration, Galloping, Parachute Suspension Lines
Abstract: Wind tunnel experiments were used to investigate the effects of geometry on the transverse galloping behavior of nominally rectangular cylinders at Reynolds numbers from 1,000 to 10,000. Static measurements of the lift and the drag forces were used to determine the variation of the normal force coefficient with angle-of-attack, in accordance with the typical quasi-steady description of galloping. Cylinders with unity chord-to-thickness ratio (side ratio) were found to vary from unstable, to neutrally stable, to stable as the corner radius was increased from sharp, to half-round, to fully round, with this effect diminishing with decreasing Reynolds number. Cylinders with side ratios of 2 or 3 demonstrated either stability over the entire Reynolds number range, or a transition from unstable to stable with increasing Reynolds number, depending on corner radius. The results demonstrated that in general, increasing the corner radius had a stabilizing effect.
Distribution Statement: 2-Distribution Limited to U.S. Government agencies only; report contains proprietary info
Acknowledged Federal Support: **Y**

Publication Type: Journal Article Peer Reviewed: Y **Publication Status:** 1-Published
Journal: International Journal of Heat and Fluid Flow
Publication Identifier Type: DOI Publication Identifier: 10.1016/j.ijheatfluidflow.2020.108721
Volume: 86 Issue: First Page #: 108721
Date Submitted: 8/31/21 12:00AM Date Published: 12/1/20 5:00AM
Publication Location:
Article Title: Effect of surface topology on the galloping instability of rectangular cylinders
Authors: Mark A. Feero, Ahmed M. Naguib, Manoochehr M. Koochesfahani
Keywords: Flow-Structure Interaction, Galloping Instability, Bluff Body Flows
Abstract: The effect of geometry on the transverse galloping instability of rectangular cylinders was studied experimentally for Reynolds numbers between 1,000 and 10,000. In particular, a comparison was made between a rectangular cylinder with rounded corners and a smooth surface, and the same baseline geometry with added surface topology synthesized from two-dimensional Fourier-modes. The effects of the topology amplitude and wavelength were investigated. From measurements of the normal (galloping direction) force coefficient variation with angle-of-attack, it was found that the added surface topology generally had a destabilizing effect relative to the smooth cylinder. At the lowest Reynolds number, the smooth cylinder was stable, while the cylinders with added topology were unstable with respect to galloping. For Reynolds numbers from 5,000 to 10,000, the added topology did not cause a similar instability.
Distribution Statement: 2-Distribution Limited to U.S. Government agencies only; report contains proprietary info
Acknowledged Federal Support: **Y**

CONFERENCE PAPERS:

Publication Type: Conference Paper or Presentation **Publication Status:** 1-Published
Conference Name: AIAA Scitech 2019 Forum
Date Received: 29-Aug-2020 Conference Date: 07-Jan-2019 Date Published: 07-Jan-2019
Conference Location: San Diego, California
Paper Title: Geometry effects on the galloping instability of rectangular cylinders at low Reynolds number
Authors: Mark Feero, Ahmed Naguib, Manoochehr Koochesfahani
Acknowledged Federal Support: **Y**

Publication Type: Conference Paper or Presentation **Publication Status:** 1-Published
Conference Name: leventh International Symposium on Turbulence and Shear Flow Phenomena (TSFP11)
Date Received: 27-Aug-2019 Conference Date: 30-Jul-2019 Date Published: 31-Jul-2019
Conference Location: Southampton, UK
Paper Title: SURFACE TOPOLOGY EFFECTS ON THE TRANSVERSE GALLOPING BEHAVIOR OF RECTANGULAR CYLINDERS
Authors: Mark Feero, Ahmed Naguib, Manoochehr Koochesfahani
Acknowledged Federal Support: **Y**

Publication Type: Conference Paper or Presentation **Publication Status:** 1-Published
Conference Name: AIAA Scitech 2020 Forum
Date Received: 29-Aug-2020 Conference Date: 06-Jan-2020 Date Published: 06-Jan-2020
Conference Location: Orlando, FL
Paper Title: Influence of surface topology on boundary layer and near-wake behavior of rectangular cylinders
Authors: Kian Kalan, Mark Feero, Ahmed Naguib, Manoochehr Koochesfahani
Acknowledged Federal Support: **Y**

RPPR Final Report
as of 18-Oct-2021

Publication Type: Conference Paper or Presentation **Publication Status:** 1-Published
Conference Name: AIAA Scitech 2021 Forum
Date Received: 31-Aug-2021 Conference Date: 11-Jan-2021 Date Published: 11-Jan-2021
Conference Location: VIRTUAL EVENT
Paper Title: Characterization of the Aerodynamics of Rectangular Cylinders with Surface Topology
Authors: Kian Kalan, Alireza Safaripour, Ahmed Naguib, Manoochehr Koochesfahani
Acknowledged Federal Support: **Y**

Partners

,

I certify that the information in the report is complete and accurate:
Signature: Ahmed M Naguib
Signature Date: 8/31/21 10:14AM

Final Report on

Mechanisms of Force and Moment Generation by the Flow over Oscillating Rectangular Cylinders

Funded by the Army Office of Research

Grant number: W911NF1710153

Performance Period: June 01, 2017 – May 31, 2021

Principal Investigators

Ahmed Naguib and Manoochehr Koochesfahani

Mechanical Engineering Department, Michigan State University, East Lansing, MI-48824

Report Date

August 31, 2021

Contents

I. Background

This document provides an account of the project's accomplishments during its full period of execution from June 1st, 2017 through May 31st, 2021.

The present investigation is motivated by understanding the flow physics leading to flow-induced vibration of suspension lines in Precision Airdrop Systems (PADS). PADS play a critical role in the US Army's ability to rapidly and accurately deliver supplies and cargo to troops. Vibration of the suspension lines influences both the overall PADS aerodynamics and the complexity and weight of the control system, adversely affecting PADS performance and capability.

This study follows in the footsteps of the work of Siefers *et al.* [1] who observed large-amplitude (few line thicknesses), low-frequency (substantially less than that of vortex shedding) vibration of a flat Dacron parachute line mounted across the height of the test section of a wind tunnel. These observations, complemented with hot-wire measurements in the wake of the line and flow visualization of a scaled-up model of the line, led the authors to hypothesize that the oscillations are due to the aero-elastic instability of galloping. It was difficult, however, for the authors to ascertain this conclusion in the absence of information regarding the aerodynamic load acting on the line.

Motivated by the findings of Siefers *et al.* [1], the present investigation is undertaken to provide basic understanding of the galloping instability characteristics of rectangular cross-section cylinders with various geometrical parameters in the Reynolds number range relevant to PADS suspension lines ($10^3 < Re_d < 10^4$, where $Re_d = U_\infty d/\nu$; U_∞ is freestream velocity, d the line thickness, and ν the fluid kinematic viscosity). Figure 1 depicts an image of a Dacron suspension line and a corresponding solid model of the line constructed by Siefers [2]. As seen from the cross-section of the solid model in Figure 1, to first order, the suspension line geometry is approximately the same as that of a rectangular cross-section cylinder having a corner radius and surface topology. It is noteworthy that galloping vibrations are typically observed in civil engineering systems; e.g. ice-coated power lines, bridge decks, and marine structures [3], where Re_d is significantly larger than that encountered by suspension lines. As such, although a wealth of information exists for galloping characteristics of rectangular sections, most of this knowledge is for the basic sharp-corner rectangular section at Reynolds numbers well outside the range of interest. There are also very few studies on the effect of the corner radius and no studies at all concerning the surface topology.

Figure 1. An image (right) and a solid model (left) of Dacron suspension line. The model image is taken from reference [2]

II. Objectives

The key goals of this project may be summarized as follows:

1. To establish the galloping instability characteristics of sharp-corner rectangular cross-section cylinders with different side ratios (i.e. chord to thickness ratios c/d; see Figure 2) in the range $1 \leq c/d \leq 3$, and Reynolds number $10^3 < Re_d < 10^4$, using measurements of the aerodynamic load on the cylinder at different angles of attack α (see Figure 2);
2. To investigate the effect of the rectangle's corner radius (r/d) and surface topology on galloping instability characteristics of the cylinders;
3. To identify cases of interest based on the outcome of parts 1 and 2, and study the aerodynamics load of these cases under dynamic (forced-oscillation) conditions;
4. To connect the observed aerodynamic load behavior, and galloping instability characteristics, under static and dynamic conditions to the underlying flow physics. This will be accomplished using Molecular Tagging Velocimetry measurements of the boundary layer resolved velocity profiles along the model's surface and the cross-stream profiles in the wake.

III. Accomplishments: Summary

The following list provides a summary of the main accomplishments during the entirety of the project. Technical details of items 1 through 3 on the list have been published in three journal and four conference papers. Interested readers may consult these publications for details of the work. For items 4 and 5 on the list, further details are given in §*IV*.

1. A new experimental setup and procedure were established to study galloping instability characteristics of rectangular cylinders having different geometrical parameters at low Reynolds number ($10^3 < Re_d < 10^4$) in a wind tunnel. This effort specifically includes:
   - Developing a new one-component high-sensitivity mean-force balance to enable measurement of the very low magnitude force encountered in the target Reynold number range. Details of the force balance is published in [4];
   - Fabricating cylinder models with provisions to enable measurement of the surface pressure distribution around the model (in addition to force measurements) [5] and [6];
   - Establishing a procedure for systematically defining, fabricating and characterizing cylinder models having surface topology [7] and [8].
2. A static-force measurement campaign was completed in the wind tunnel to characterize the plunge galloping instability for rectangular cylinders with various geometrical features, including r/d, c/d and surface topology. The bulk of the force measurement results have been published in [5-8];
3. A measurement campaign was completed in a $15\ cm \times 15\ cm$ water tunnel to examine the effect of surface topology on the boundary layer and the wake flow of rectangular cylinders. The experiments, which utilized one-component Molecular Tagging Velocimetry (1c-MTV), were undertaken in order to understand the flow physics leading to the observed force characteristics documented in the wind tunnel experiments described in item 2 above. The main findings from the MTV measurements are published in AIAA SciTech 2020 and 2021 conference proceedings [9] and [10]. Additional findings are the subject of an AIAA SciTech 2022 abstract that is currently under review;
4. A set of experiments was completed in a larger $60\ cm \times 60\ cm$ water tunnel to study the unsteady force characteristics of harmonically heaving rectangular cylinders. The geometry of the models

examined was selected based on the outcome of the study described in item 2 above. Key findings from this part of the study are summarized in §*IV.A*;

5. 1c-MTV experiments complementing the force measurements in item 4 were carried out on the heaving cylinders. Results from these experiments uncovered non-quasi-steady behavior of the separated shear layer, leading to hypotheses regarding the connection between this behavior and galloping instability of the cylinders. Highlights of the findings from the 1c-MTV experiments can be found in §*IV.B.*

IV. Accomplishments: Details

Figure 2 depicts the configuration, the coordinate system and the parameter definitions of the present flow problem. Given the parameter definitions in the figure's caption, it is well known, e.g. see [3], that the necessary condition for plunge galloping instability (i.e. for the cylinder to be susceptible to self-sustained oscillation in the cross-stream direction) is:

$$\frac{\partial C_y}{\partial \alpha}|_{\alpha=0} > 0, \qquad [1]$$

where C_y is the coefficient of the force component in the vibration, y, direction:

$$C_y = \frac{F_y}{\frac{1}{2}\rho U_\infty^2 d b}, \qquad [2]$$

with b being the span of the cylinder. If the condition given by Equation [1] is satisfied, gallop oscillation will occur if the non-dimensional flow velocity (aka reduced velocity) U_r exceeds the critical value

$$U_{r,critical} = \frac{U_{\infty,critical}}{f_y d} = \frac{4m(2\pi\zeta)}{\rho d^2}\frac{1}{\frac{\partial C_y}{\partial \alpha}|_{\alpha=0}}, \qquad [3]$$

where f_y is the oscillation frequency, m the effective cylinder mass (including the apparent mass of the fluid), and ζ the mechanical damping ratio.

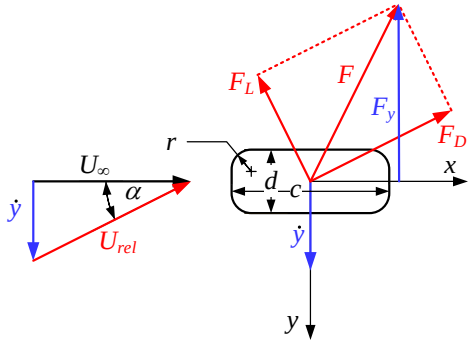

Figure 2. A schematic of the present flow configuration depicting an oscillating rectangular cylinder exhibiting plunge gallop oscillations (translation oscillation in the cross-stream direction). The relevant parameters are defined as follows: U_∞ is the freestream velocity, d cylinder thickness, c chord length, r corner radius, x streamwise direction, y cross-stream direction, F force vector, F_D drag force, F_L lift force, F_y force component in the oscillation (cross-stream) direction, U_{rel} freestream velocity *relative* to the cylinder, and α angle of attack (AoA).

Based on Equation [1], to assess whether a cylinder with a particular cross section is unstable to galloping, the variation of C_y with angle of attack (AoA) needs to be determined in order to obtain the slope $\partial C_y/\partial \alpha$

at $\alpha = 0$. If this slope, or instability parameter, is positive then the cylinder is prone to galloping. It is also noteworthy that if this slope has large magnitude, per Equation [3], the critical velocity becomes small and the cylinder would be prone to oscillation over a larger range of flow velocities.

Based on the above, the majority of the project's work during the first two years focused on obtaining the force characteristics for stationary rectangular-section cylinders with different geometrical parameters. This information is used to determine the galloping instability characteristics of these cylinders and how they are affected by the corner radius (r/d), side ratio (c/d) and the surface topology. During the third year of the project, the primary focus was on conducting high-resolution 1c-MTV measurements to characterize the boundary layer behavior around selected cylinder model geometries with/without surface topology. The results from both the force and velocity measurement efforts have been published in a number of manuscripts [4-10], and hence their details are left out of this report (although the associated conclusions are summarized in §*V*). The remainder of this section is thus focused on summarizing the key results and findings from the oscillating-cylinder experiments. The outcome of this effort has not been published elsewhere as it involves a great amount of data obtained in the last year of the project.

IV.A. Dynamic Force Measurement Results

One of the main goals of the present project is to assess the applicability of the quasi-steady assumption traditionally employed in analyzing galloping instability. This assessment was initially motivated by the observation in [1] that a suspension line mounted in the wind tunnel could exhibit vibrations as large as a few line thicknesses. It is suspected that such unusually large vibration amplitude could lead to the invalidity of the quasi-steady hypothesis. Surprisingly, as will be seen below, our dynamic force measurements show that a significant non-quasi-steady behavior is already observed for cylinders oscillating with an amplitude even smaller than the cylinder thickness! These observations suggest that this unexpected non-quasi-steady effect is a creature of the low Reynolds number range of interest, which has been rarely addressed in the literature. Accordingly, our experimental plan for studying oscillating cylinders were focused on the low-amplitude non-quasi-steady cases.

To narrow down the cases examined under unsteady motion, the static force results are employed. The cases selected are unstable to galloping for part of, or the full Reynolds number range investigated: the sharp corner cylinders with $c/d = 2$ and 3, and their fully-round counterpart ($r/d = 0.5$). In this report, we focus only on the sharp-corner $c/d = 2$ case, where the cylinder is unstable to galloping over $1{,}000 \leq Re_d \leq 10{,}000$. All experiments are conducted in the closed-return $60\ cm \times 60\ cm$ water tunnel, where an ATI Mini-40 6-component load cell is available for conducting unsteady load measurements. The cylinder model is attached to the load cell, which in turn is connected to a rotary servo motor fixed to a linear servo stage. The rotary motor is used to change the angle of attack of the cylinder. This is only done when conducting static force measurements. For dynamic force measurements, the cylinder is fixed at zero geometrical angle of attack and the linear servo stage is used to oscillate the cylinder in the cross-flow direction (i.e. heave oscillations). The cylinder thickness d is 34 mm, and the aspect ratio is 16. The aspect ratio and the geometrical blockage of 5% have the same values as those used in the wind-tunnel static-force measurements. However, the water tunnel streamwise velocity turbulence intensity of 1.9% and 0.3%, with and without unsteadiness due to slushing respectively, is larger than that of the wind tunnel (0.1%). In addition, the diameter of the cylinder's end plate for the dynamic tests ($d_{EP}/d = 6$; sized based on literature) is smaller than $d_{EP}/d = 15$ used in the wind tunnel experiments. Figure 3 shows a schematic of the water-tunnel setup.

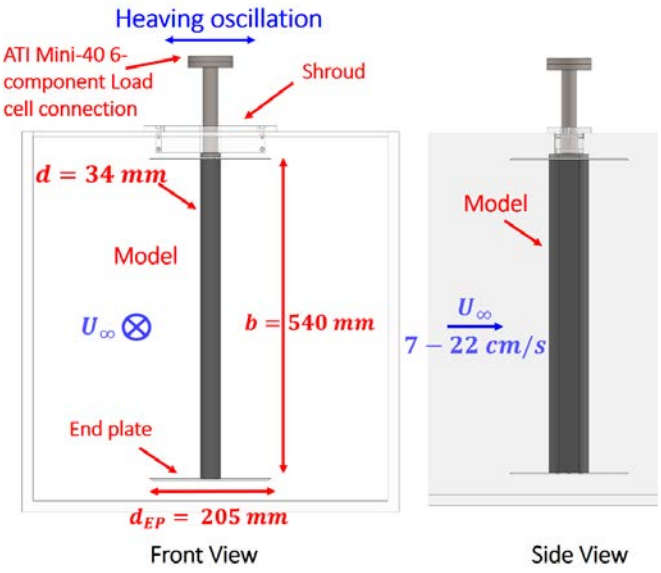

Figure 3. Schematic of the setup in the water tunnel for investigating the unsteady force acting on heaving rectangular cylinders. Flow is into the page in the left (front) view. The shroud shields the shaft connecting the cylinder model to the load cell from the main stream.

For all experiments two oscillation amplitudes are considered: $A_y^* = A_y/d = 0.2$ and 0.5, and for a given Reynolds number (i.e. freestream velocity U_∞), the reduced velocity $U_r = U_\infty/df_y$ is varied between 30 and 500 by changing the oscillation frequency f_y between 0.22 and 0.004 Hz respectively. Note that this U_r range is larger than the vortex shedding reduced velocity U_{rv} encountered with the present model (between 11 and 15). Thus, from current understanding of galloping, the oscillation parameters should correspond to quasi-static conditions. It is generally accepted (e.g. [3]) that quasi-steady oscillations occur for $U_r > 20$. Also, significantly, when studying the effect of the oscillation amplitude and/or the Reynolds number, the effective angle of attack amplitude α_o is kept fixed. To keep α_o constant when changing A_y^* and Re_d, the parameter $U_r/(A_y/d)$ is maintained unchanged.

Prior to looking at the oscillating-cylinder results, it was desired to verify that the basic galloping instability characteristics are unchanged between the wind and the water tunnel tests. To this end, the static $C_y - \alpha$ data from both facilities are compared in Figure 4 for the $c/d = 2$ and $r/d = 0$ model at the two Reynolds number considered: $Re_d = 2{,}500$ and $Re_d = 7{,}500$. Note that one of these Reynolds numbers falls into, what we call the "low", and the other into the "high" Reynolds number range. In both cases, the wind tunnel results at $Re_d = 10{,}000$ are also provided as a common reference. Focusing on the $Re_d = 2{,}500$ case (left plot in Figure 4), a significant change in the slope of the $C_y - \alpha$ curve at zero angle of attack is seen between the wind and the water tests. However, both cases exhibit instability to galloping with the water tunnel case being more prone to galloping by virtue of the steeper slope (corresponding to lower critical reduced velocity). Interestingly, the water tunnel data at $Re_d = 2{,}500$ are very similar to those obtained in the wind tunnel at the higher Reynolds number of 10,000. A plausible reason for this similarity is the higher freestream turbulence level in the water tunnel, which could hasten the laminar-turbulence transition in the separated shear layer around the model, causing the flow to effectively behave as a higher Reynolds number flow in a quieter environment.

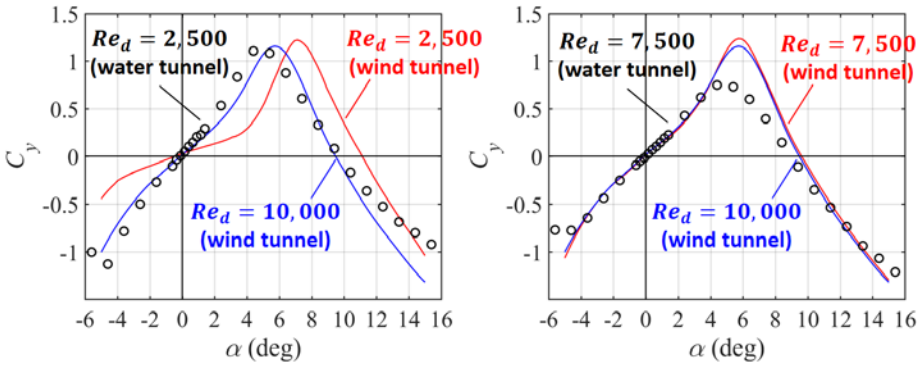

Figure 4. Comparison between the static $C_y - \alpha$ characteristics obtained in the wind and the water tunnel facilities at $Re_d = 2,500$ (left) and 7,500 (right) for the sharp-corner rectangular cylinder with $c/d = 2$.

On the other hand, at $Re_d = 7{,}500$, the wind and the water tunnel results agree very well over the approximate range $-3 \leq \alpha \leq 3$. Thus, the basic galloping instability characteristics are practically identical for both models. However, significant differences are seen near the maximum of C_y. This only affects the angle at which the cylinder becomes stable to galloping, which occurs at a smaller angle of attack in water. Overall, for both Reynolds numbers, the cylinder geometry considered remains unstable to galloping in water, as deduced from the earlier wind-tunnel experiments.

The dynamic cylinder results are shown in Figure 5, which is organized to show the Reynolds number effect along rows (comparing left to right plots) and the amplitude effect along columns (comparing top to bottom plots). In each of the four plots shown, the phase-averaged C_y measured during oscillation is plotted against the effective angle of attack. The different-colored solid lines correspond to different values of U_r/A_y^*, as shown in the legend, along with the corresponding U_r values. Since A_y^* is fixed for a given plot, the cases corresponding to different lines are obtained by changing the oscillation frequency, with the oscillation frequency *increasing* with *decreasing* U_r. Each plot also includes a dashed black line connecting circular symbols which represent the static $C_y - \alpha$ data.

The key point in examining the results in Figure 5 is the applicability of the quasi-steady hypothesis for the oscillation conditions examined. Specifically, if quasi-steadiness is valid, then the phase-averaged $C_y - \alpha$ results should collapse on the static characteristics. Focusing on the plot in the top-left corner of Figure 5 ($Re_d = 2{,}500$ and $A_y/d = 0.2$), a large deviation is observed between the dynamic and the static force results at low reduced velocities. The deviation manifests itself in the form of a hysteresis loop that becomes smaller with increasing U_r (reducing oscillation frequency) while approaching, but not fully collapsing on, the static characteristics. The presence of the hysteresis loop in itself is not too surprising and could be attributed (at least in part) to the presence of *irrotational added-mass force* and other forces that are proportional to the cylinder's acceleration ($\ddot{y}$) and/or displacement. These forces are not important to galloping instability since they are $\pi/2$ out of phase of the cylinder's velocity ($\dot{y}$), and hence impart zero net mechanical work to the cylinder over an oscillation cycle. Thus, *if these forces are the sole cause* for the deviation from non-quasi-steadiness in Figure 5, then the present results do not invalidate the applicability of quasi-steady analysis of galloping as far as the net effect over an oscillation cycle is concerned.

Figure 5 also shows that the deviation between the dynamic and the static force characteristics becomes smaller with increasing Reynolds number and amplitude. For the same oscillation amplitude, increasing the Reynolds number decreases the size of the dynamic-force loop at the same value of U_r (i.e. comparing plots

with the same line color between the left and right columns in Figure 5). A similar trend is observed for increasing the amplitude at the same Reynolds number, as seen from the smaller $C_y - \alpha$ loops in the bottom plots compared to those on the top. This amplitude effect should be treated with caution, however, since the same line color in the top and bottom plots indicates the same AoA, and not displacement, amplitude. As stated earlier, under this condition when changing A_y^*, U_r/A_y^* remains unchanged. Hence, increasing A_y^* is accompanied by a proportional increase in U_r (i.e. reduction in the oscillation frequency). Therefore, it is not possible to ascertain if the smaller deviation from quasi-steadiness is due to the increased amplitude or reduced frequency. If one is to examine A_y^* effect when U_r is kept fixed, the results show that increasing A_y^* causes larger deviation between the dynamic and the static force. This can be seen from comparing the magenta-colored line in the top plots of Figure 5 to the dotted-blue line in the bottom plots; both of which are at $U_r = 100$. Overall, Figure 5 shows that the case having the higher Reynolds number and amplitude (the lower-right corner plot in Figure 5) has the smallest deviation from the static-force characteristics.

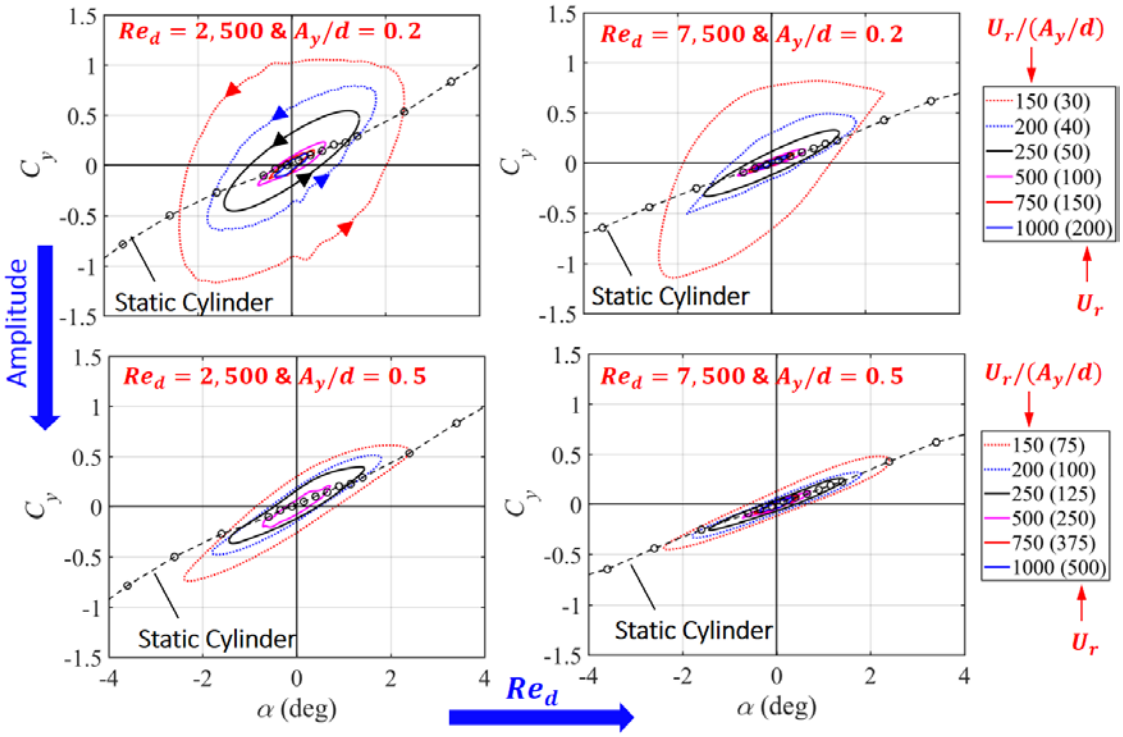

Figure 5. Dynamic-force measurements for $A_y/d = 0.2$ (top) and 0.5 (bottom), and $Re_d = 2,500$ (left) and 7,500 (right) of the sharp-corner cylinder with $c/d = 2$. Solid lines depict a plot of the phase-averaged force coefficient versus the angle of attack at different phases of the oscillation cycle. Different colors correspond to different values of $U_r/(A_y/d)$ and U_r. The arrows shown on some of the lines in the top-left plot indicate the direction of progression of the force coefficient during the oscillation cycle. All lines in the figure follow the same direction. The cases corresponding to $U_r = 375$ and 500 are not carried out for $Re_d = 2,500$ since they require prohibitively long time to run. The black circles connected with broken black line represent the static-force coefficient.

Based on the above, two key questions arise:

1. Is the deviation from quasi-steady behavior in Figure 5 completely benign for galloping instability? Or, are there non-quasi-steady effects on the force driving galloping?

2. How can one determine the equivalent of the galloping instability parameter $\partial C_y/\partial\alpha|_{\alpha=0}$ in the presence of the $C_y - \alpha$ loop?

We first address the second question by introducing an energy-based definition of the galloping instability parameter. As discussed in §*VI*, galloping instability is determined from the slope of $C_y - \alpha$ curve at the origin. Under quasi-steady conditions, this slope is determined form the static-model tests and, for small-amplitude galloping oscillations, the $C_y - \alpha$ behavior may be linearized as shown in Figure 6 (left). Also, for such small oscillations, $\alpha = \tan^{-1}(\dot{y}/U_\infty) \approx \dot{y}/U_\infty$, so that the linear $C_y - \alpha$ behavior is effectively the same as $C_y - \dot{y}/U_\infty$, and if the slope of the line is positive, it corresponds to a cylinder unstable to galloping. It is easy to show that the corresponding plot, but on force-displacement, rather than force-velocity diagram, would describe an ellipse that tracks in the clockwise direction (the red line in Figure 6, right) which indicates energy transfer from the flow to the cylinder (i.e. the cylinder that is unstable to galloping). The area of this ellipse is numerically equal to the magnitude of the work done per cycle on the cylinder, with the area becoming larger with increasing slope of the $C_y - \alpha$ line. Conversely, a stable cylinder would possess a negative-sloped $C_y - \alpha$ line, as shown by the dashed black line in Figure 6 (left). If the magnitude of the slope of this line is the same as the red line then the corresponding ellipses of both lines coincide on the $C_y - y/d$ diagram, but with the cylinder oscillation traversing the ellipse in two opposite directions.

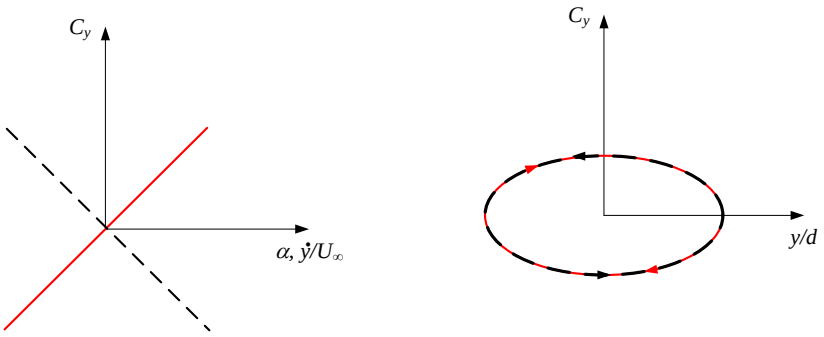

Figure 6. Comparison of C_y characteristics plotted versus cylinder velocity and angle of attack (left) with those plotted versus cylinder displacement (right): unstable (solid red line) and stable (broken black line) cylinders.

The non-dimensional work done on the cylinder over one oscillation cycle (area of the ellipse on the $C_y - y/d$ diagram) is computed using:

$$W^* = \frac{W}{\frac{1}{2}\rho U_\infty^2 d^2 b} = \frac{\oint F_y dy}{\frac{1}{2}\rho U_\infty^2 d^2 b} = \oint C_y dy^* \qquad [4]$$

where b is the cylinder span and $y^* = y/d$. It is easy to show that the slope of the line on $C_y - \alpha$ diagram is connected to W^* by the following equation:

$$\frac{\partial C_y}{\partial \alpha}|_{\alpha=0} = \frac{W^*}{2\pi^2\left(\frac{A_y^*}{U_r}\right)A_y^*} \equiv a_g, \qquad [5]$$

where a_g is used to denote the galloping instability parameter. Thus, it is possible to connect the traditional galloping instability parameter $\partial C_y/\partial\alpha|_{\alpha=0}$ to the work done on the cylinder per cycle W^*. If W^* is positive, the cylinder is unstable to galloping and vice versa. The advantage of this energy-based instability criterion is that the presence of added-mass effects, or other forces that are proportional to the cylinder

displacement or acceleration will only cause rotation of the principle axes of the ellipse on $C_y - y/d$ diagram but not change the area of the ellipse. Similarly, if the force behavior is non-linear with angle of attack, the resulting higher harmonics in the force oscillation, do not contribute to the net work done on the cylinder at the imposed oscillation frequency (due to orthogonality of different harmonics). Hence, these higher harmonics will distort the shape of the ellipse but not change its net area. It can also be shown that the relation given by Equation [5] is applicable to non-quasi-steady oscillation as well.

Given the above, we proceed to answer the first of the two questions posed earlier by computing a_g for the oscillating cylinder and comparing it to a_{gs} of the static cylinder. The calculation is done for the same cases considered in Figure 5 while excluding cases where the phase-averaged force history is not clearly distinguishable from the cycle-to-cycle variation in the force oscillation. This scenario primarily occurs for the largest values of U_r/A_y^* of 750 and 1,000, where the oscillation frequency is the smallest, resulting in larger drift uncertainty in force measurements, and $\alpha_o < 0.5°$, resulting in weak periodic force oscillation.

The computed a_g values are plotted versus U_r/A_y^* in Figure 7 (left) and against U_r in Figure 7 (right). The plots include two broken lines corresponding to a_{gs} values for $Re_d = 2{,}500$ (red), and 7,500 (blue). Figure 7 (left) shows that galloping instability is affected by the motion of the cylinder; i.e. *the galloping instability exhibits non-quasi-steady influences*. The influences lead to increased instability relative to quasi-steady analysis. For a given case (given Reynolds number, as indicated by the symbol color, and oscillation amplitude, as given by the symbol shape and fill), the deviation from the quasi-steady instability parameter increases with decreasing U_r/A_y^* (i.e. with increasing the angle of attack amplitude α_o). One exception is at the lower oscillation amplitude and Reynolds number (red open circles), where this monotonic trend is reversed for the smallest U_r/A_y^* values. For a given amplitude (symbol shape) increasing the Reynolds number causes a_g to be closer to a_{gs} (except for the one case noted already), and for a given Reynolds number (symbol color), increasing the oscillation amplitude (but for the same α_o as discussed earlier) moves a_g towards the quasi-steady value.

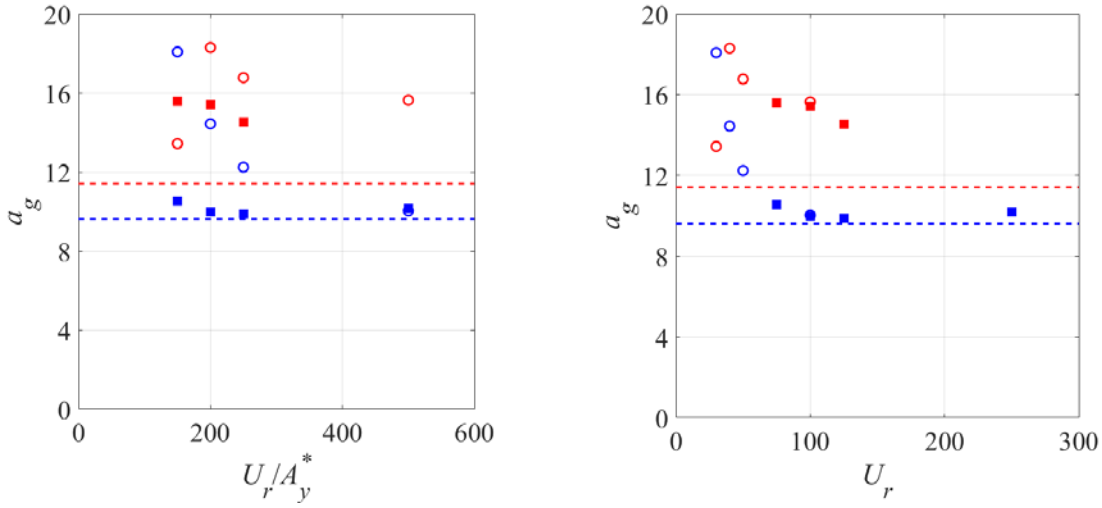

Figure 7. Dependence of the galloping instability parameter on U_r/A_y^* (left) and U_r (right) for two different oscillation amplitudes and Reynolds numbers: $Re_d = 2,500$ (red) and $7,500$ (blue), and $A_y^* = 0.2$ (open circles) and 0.5 (closed squares). Broken lines indicate the quasi-steady galloping instability parameter with their color indicating the Reynolds number.

The results in Figure 7 (left) for the different cases do not exhibit any collapse when plotted versus U_r/A_y^*. In contrast, when a_g is plotted versus U_r (Figure 7, right), an apparent collapse of the data for a given Reynolds number is observed. With the notable exception of the one case mentioned above, the collapse is such that a_g systematically approach a_{gs} with increasing U_r. Since U_r is inversely proportional to the frequency of oscillation, the results are commensurate with the expectation that as the oscillation frequency becomes slower, the force behavior will become increasingly quasi-steady. However, the approach towards quasi-steadiness with increasing U_r is significantly slower at the lower Reynolds number, where even for values of U_r as high as 150, a significant deviation from quasi-steadiness persist. This value is almost eight-fold that quoted in textbooks ($U_r > 20$) for quasi-steady galloping conditions to be established.

The above results indicate that the deviation from quasi-steady behavior correlates with the reduced velocity rather than the effective AoA amplitude. In turn, this suggests that with increasing frequency, the ability of the flow to keep up with the imposed oscillation decreases and this ability is reduced further with decreasing Reynolds number. This Reynolds number dependence may be a simple manifestation of the change in the boundary layer thickness rather than something more complex, such as a modification of the instability of the separated shear layer. Proceeding with the first idea and considering the characteristic viscous time scale T_v for a boundary layer with thickness δ:

$$T_v = \frac{\delta^2}{\nu} \sim \frac{d^2}{\nu\, Re_d}, \qquad [6]$$

or, for two different Reynolds numbers,

$$\frac{T_{v1}}{T_{v2}} = \frac{Re_{d2}}{Re_{d1}} \qquad [7]$$

Equation [7] shows that the characteristic boundary layer response time at a higher Reynolds number is faster than that at a lower Reynolds number in proportion to the Reynolds number ratio. This is qualitatively consistent with the above observation showing a_g approaching to the quasi-steady value with increasing U_r at $Re_d = 7{,}500$ faster than at $Re_d = 2{,}500$. Furthermore, this alludes to the possibility of better collapse with Reynolds number in the data in Figure 7 (right) if a_g is plotted versus $U_r Re_d$. This is done in Figure 8, where a_g is normalized by a_{gs}, to account for the different values of a_{gs} at different Reynolds numbers. In this plot, the quasi-steady condition is defined by the broken black line, where $a_g/a_{gs} = 1$. Inspection of the plot shows that, while there is no complete collapse of the data at different Reynolds numbers on a common curve, the approach towards quasi-steady behavior with increasing U_r for both Reynolds numbers appears to happen equally fast when plotted versus $U_r Re_d$. Whether this approach towards quasi-steadiness does indeed collapse on a single curve, would require data at intermediate Reynolds numbers between 2,500 and 7,500 (which were not compiled in this project). The plot in Figure 8 also indicates that a_g/a_{gs} reaches approximately unity beyond a value of $U_r Re_d = 10^6$. This explicitly demonstrates the required higher U_r (slower oscillation frequency) value to reach quasi-steady conditions as the Reynolds number is decreased.

Another notable observation from Figure 8 is the absence of data collapse at different Reynolds numbers in the limit $U_r Re_d \to 0$. This suggests that the dynamics of the boundary layer in that limit are becoming more complex, involving time scales other than the boundary layer viscous time scale (likely connected with the dynamics of the shear layer separation/reattachment and possible interaction with the wake).

As indicated earlier, of all the data presented in Figures 7 and 8, one case does not follow the general trends discussed above. This point, which is found at the lowest Reynolds number and reduced velocity (left most open red circle), appears to indicate that if U_r is sufficiently reduced (i.e. the frequency of oscillation is sufficiently increased), it is possible to also return to quasi-steady conditions. From a physical point of

view, this point does not make sense, and as will be seen in the next section where we consider 1c-MTV characterization of the unsteady boundary layer, this case departs significantly from quasi-equilibrium conditions. The boundary layer data will also allow us to propose a different interpretation of the decrease in a_g/a_{gs} for this "anomalous" case.

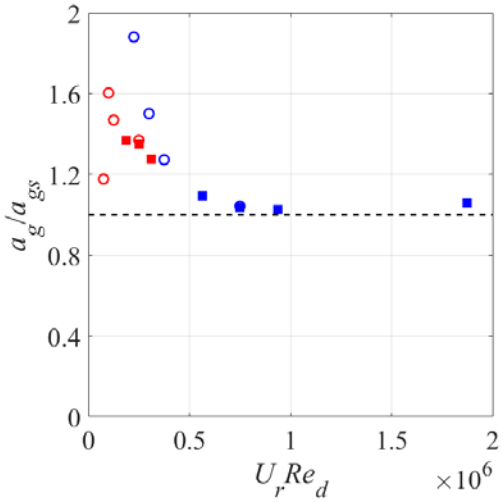

Figure 8. Dependence of galloping instability parameter on $U_r Re_d$ for two different oscillation amplitudes and Reynolds numbers: $Re_d = 2,500$ (red) and $7,500$ (blue), and $A_y^* = 0.2$ (open circles) and 0.5 (closed squares). Broken line indicates the quasi-steady galloping instability parameter.

IV.B. Characterization of the Boundary Layer on the Oscillating Cylinder

1c-MTV measurements are conducted on one side of the cylinder during forced oscillation and the results are phase-averaged relative to the oscillation cycle. The measurement side is labeled "top" when the angle of attack of the static model and the effective angle of attack of the moving model is positive. Conversely, if the AoA is negative, the measurement side is referred to as the "bottom" surface of the cylinder. Measurements are conducted for a few selected cases of those used in force measurements. Before discussing MTV results, the reader is referred to Figure 9 for orientation regarding the known behavior of boundary layer separation and reattachment on a static square cylinder and the connection of this behavior to the instability to galloping. Similar qualitative behavior is known to occur for rectangular cylinders with side ratios between 1 and 3; a range that encompasses the present geometry ($c/d = 2$). As seen from Figure 9, at zero AoA, two symmetric open separation zones are formed from boundary layer separation on the top and bottom front corners of the cylinder. As the angle of attack increases, the lower shear layer curves towards the model, causing a reduction in surface pressure, while the top shear layer moves away from the surface. The net effect is a downward (positive) vertical force (F_y), indicating an increase in F_y with α; i.e. instability to galloping. With further increase in the angle of attack, and further curvature of the bottom shear layer towards the surface, this trend continues until the shear layer reattaches on the bottom surface. This is the point at which F_y reaches its maximum value. Further increase in α causes movement of the reattachment point upstream and an associated increase in the pressure on the bottom surface downstream of reattachment. The net result is a reversal in the trend of F_y with α, so the cylinder becomes stable to galloping beyond the point of reattachment of the shear layer on the bottom surface.

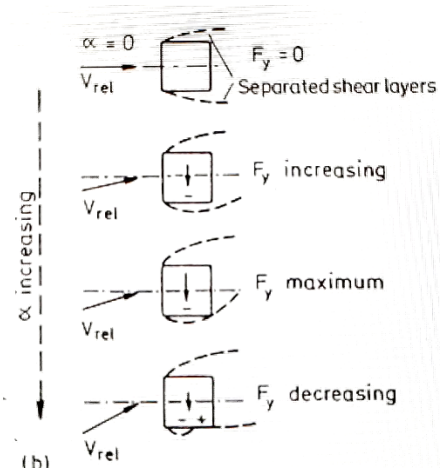

Figure 9. Separated shear layer and galloping force behavior with increasing angle of attack for a square cylinder. Taken from [11]

Examination of the 1c-MTV results on the moving cylinder reveals a shear layer behavior versus the effective angle of attack that is qualitatively similar to that of the static cylinder. However, the motion of the cylinder causes the shear layer movement towards and away from the surface on the bottom and top sides of the cylinder, respectively, to be larger than for the static cylinder. This can be seen in Figures 10a and 11a for $Re_d = 2{,}500, A_y^* = 0.2$ and $U_r/A_y^* = 150$ (the anomalous case discussed in the previous section). The first of these figures shows a color map of the streamwise velocity at the motion phase where the shear layer is closest to the bottom surface of the cylinder (recall that the measurement side is the "bottom" surface when $\alpha < 0$) compared to the static counterpart at the same angle of attack. The second figure shows similar plots but for the motion phase where the shear layer is displaced farthest from the cylinder on the top surface. The most striking difference between the moving and static cylinders is seen in Figure 10a where the shear layer on the bottom has not only reattached but also moved a short distance upstream of the aft corner. In contrast, the bottom shear layer on the static model is seen to remain open. In fact, based on the static-model force measurements (Figure 4), reattachment does not occur until $\alpha \approx 4.5°$, almost twice the oscillation amplitude of the moving cylinder $\alpha_o = 2.4°$! Similarly, Figure 11a depicts the farther excursion of the shear layer from the top surface during the motion in comparison to the static cylinder. To aid the reader in seeing this effect, which is not as obvious as in the case of the bottom shear layer, a dashed black line is drawn horizontally to mark where an arbitrarily chosen contour (yellow) meets the end of the measurement domain for the static cylinder. The corresponding contour for the oscillating cylinder clearly overshoots this line.

Considering similar comparison but for the higher Reynolds number of 7,500, similar qualitative behavior is seen in Figure 10b and 11b for the bottom and the top shear layer respectively. Interestingly, when the shear layer is closest to the bottom surface (Figure 10b, left), it reattaches, or is very close to reattaching, on the aft corner. Comparing this to Figure 10a (left) for $Re_d = 2{,}500$, where the reattachment point has moved slightly upstream of the aft corner, this indicates that the lower Reynolds number deviates more from the static condition (open separation zone) than the higher Reynolds number, which is consistent with the force measurements. More significantly, this shows that the anomalous low Reynolds number case is indeed far from quasi-static conditions, opposite to what force measurements suggest from the reduction of a_g towards the quasi-steady value when U_r/A_y^* is reduced from 200 to 150 (U_r reduced from 40 to 30) in Figure 7. Moreover, by drawing an analogy with the $F_y - \alpha$ behavior described for the static cylinder in Figure 9, it appears that this reduction in a_g is likely a reflection of a decrease in the galloping force due to

the movement of the reattachment point upstream of the aft corner. If true, this would imply if data are acquired for $Re_d = 7{,}500$ and $A_y^* = 0.2$ (blue open circles in Figure 7, right) at a lower U_r value than the smallest value shown in Figure 7 (right), a drop in a_g would be observed as well. Unfortunately, no data were acquired for this condition.

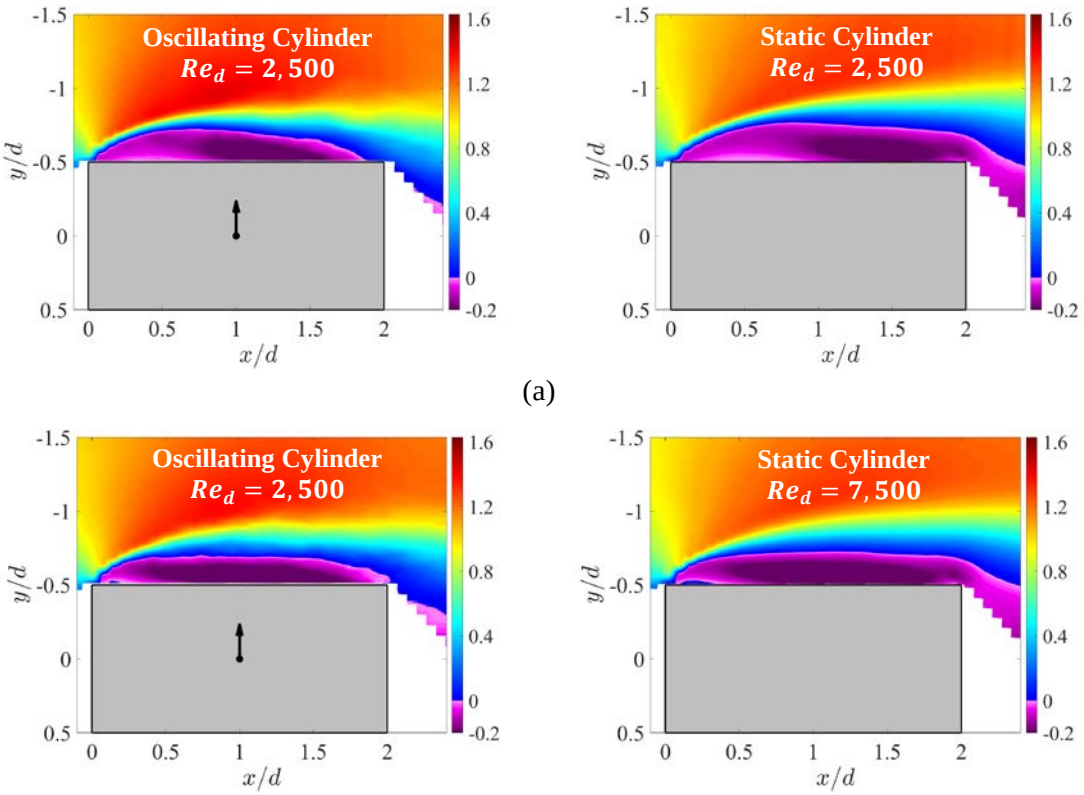

Figure 10. Effect of Reynolds number on quasi-steadiness of the streamwise velocity u field for $A_y^* = 0.2, U_r/A_y^* = 150$: (a) $Re_d = 2,500$, (b) $Re_d = 7,500$. Results for the oscillating (left) and the static (right) cylinder are shown at $\alpha = -2°$, when the shear layer moves closest to the "bottom" surface of the moving cylinder. Color indicates u/U_∞ value with purple highlighting the reverse flow region. Flow is from left to right.

Another instructive comparison to consider is the influence of the reduced velocity on the separated shear layer behavior. Based on force measurements, it was concluded that as U_r increases the galloping instability parameter approaches that based on quasi-steady analysis. With the MTV data, it is possible to confirm that this trend is also reflected in the behavior of the shear layer. This is demonstrated for $Re_d = 2{,}500$ and $A_y^* = 0.2$ in Figure 12, where the bottom shear layer behavior is compared for two different values of U_r at an effective angle of attack of $-1°$. The figure also includes results for the static cylinder at the same angle of attack. The plots clearly demonstrate the increasing proximity to quasi-steady conditions with increasing U_r. At $U_r = 30$, the shear layer is seen to reattach very close, if not at the aft corner of the cylinder, in comparison to an open separation bubble for the static case. As U_r is increased to $U_r = 50$, the bubble becomes open, similar to the static cylinder, but overall the shear layer appears to be closer to the surface than in the static case. These results are consistent with the galloping instability parameter behavior with U_r observed earlier.

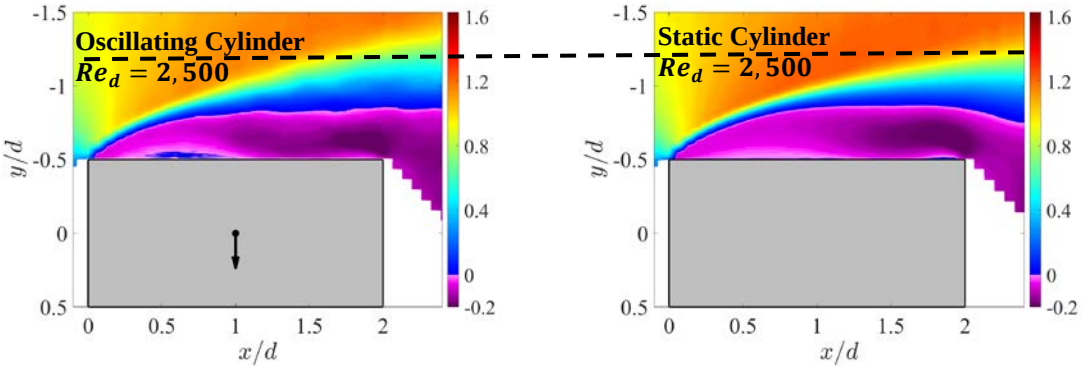

(a)

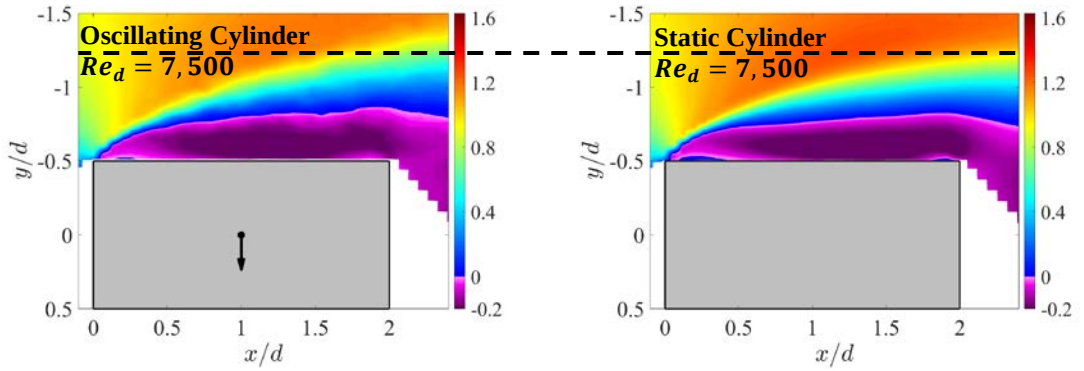

(b)

Figure 11. Effect of Reynolds number on quasi-steadiness of the streamwise velocity u field for $A_y^* = 0.2, U_r/A_y^* = 150$: (a) $Re_d = 2,500$, (b) $Re_d = 7,500$. Results for the oscillating (left) and the static (right) cylinder are shown at $\alpha = 2°$, when the shear layer is farthest from the "top" surface of the moving cylinder. Color indicates u/U_∞ value with purple highlighting the reverse flow region. Flow is from left to right.

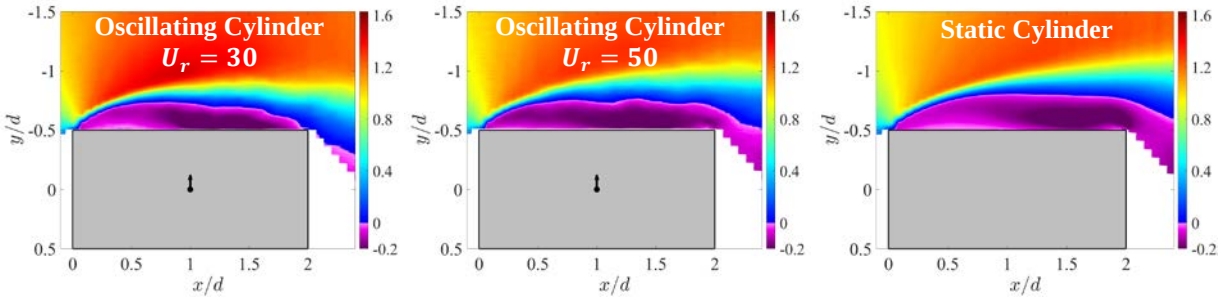

Figure 12. Effect of the reduced velocity on quasi-steadiness of the streamwise velocity u field at $Re_d = 2,500$ and $A_y^* = 0.2$: $U_r = 30$ (left), $U_r = 50$ (center), and static (right) cylinder at $\alpha = -1°$. Purple color indicates reverse flow. Color indicates u/U_∞ value with purple highlighting the reverse flow region. Flow is from left to right.

V. Conclusions

Key conclusions drawn from the project's results are summarized in the following sections. The conclusions include those from results not included in this report but published elsewhere [4-10] as well as those discussed in §*V*.

V.A. Reynolds Number Effect on Galloping Instability

The mean aerodynamic force characteristics and the galloping instability of rectangular cylinders can exhibit a fundamental change across $Re_d \approx 5{,}000$. Hence, the range $Re_d < 5{,}000$ is referred to as the "low" Reynolds number region, and that above $5{,}000$ as the "high" Reynolds number zone. This difference between low and high Reynolds number behavior is found for a cylinder side ratio at which the cylinder is known to be stable to galloping in literature. The change in behavior from the high to the low Reynolds number is characterized by:

- A flip in the galloping stability from stable at high Reynolds number to unstable at low Reynolds number;
- The flip in galloping stability is correlated with how the shear layer reattachment on the "bottom" cylinder surface changes with angle of attack, and associated change in the separation-zone pressure on the "top" surface. The behavior of these flow features is found to be different below $Re_d = 5{,}000$ from that above.

V.B. Surface Topology Effect on Galloping Instability

Idealized "Fourier surface topology" with comparable characteristics (non-dimensional amplitude and wavenumbers) to that of PADS suspension lines could have a pronounced effect on galloping instability. Specifically:

- Topology can cause the cylinder to become unstable to galloping in the "low" Reynolds number range;
- Topology results in "flatter" $C_y - \alpha$ curves, making the cylinder less prone to hard galloping;
- Topology amplitude has stronger influence on the mean force and galloping characteristics than the topology wavenumber (within the limited range of parameters investigated);
- If surface topology is unavoidable, larger (10% amplitude) topology has more favorable characteristics for galloping resistance than smaller (5% amplitude) topology.

V.C. Effect of Surface Topology on Boundary Layer Characteristics

Analysis of 1c-MTV velocimetry data sets leads to the hypothesis that the effect of the surface topology on galloping stability of rectangular cylinders is primarily driven by the topological features along the leading edge (LE). The details of the topology along the sides and in the wake are of secondary importance. Of particular significance is the role of the leading-edge topology in causing early separation on the top surface of the cylinder when a topology peak is present at the LE. Additionally, it is found that the topology may act as a streamwise vortex generators, to delay and weaken the stall peak for geometries that are stable to soft galloping, and hence act as a lifting body. The former topology effect is most significant to soft galloping and the latter to hard oscillation. Additional studies incorporating both force and boundary layer measurements at several Reynolds numbers are needed to specifically assess the validity of these ideas.

V.D. Effect of Surface Topology on Wake Behavior

An ongoing analysis of 1c-MTV data of the wake of the cylinders with and without surface topology shows close connections between the boundary layer behavior and subsequent development of the wake flow. Results when a topology peak is present at the LE at $Re_d = 1{,}100$ show that the protrusion of the topology into the flow is associated with earlier boundary layer separation and a wider near wake than in the case of the smooth cylinder. Spanwise variation of the topology reduces the initial wake width, presumably due to the streamwise vortex generation effect indicated in §*V.C*. The leading-edge separation also seems to lead

to less organized vortex shedding in the wake. Overall, the data show that as the initial wake width increases, the shedding Strouhal number decreases, wake vortex formation appears to occur closer to the cylinder, and the peak level of velocity fluctuations increases. It is evident that the surface topology can alter the wake structure significantly. This alteration could have important practical ramifications when considering flow-induced vibration of PADS suspension line systems, where the wakes of the upstream lines impinge on those downstream. For these problems it will be important to also understand the time-dependent characteristics of the wake, which we are presently exploring and is the subject of an AIAA SciTech 2022 under review.

V.E. Assessment of Quasi-Steady Behavior During Forced Cylinder Oscillations

Both force and boundary- layer resolved measurements on rectangular cylinders exhibiting forced harmonic oscillations have demonstrated a breakdown in the quasi-steady behavior within the Reynolds number range relevant to PADS. The deviation from quasi-steadiness becomes stronger with decreasing Reynolds number and reduced velocity (increasing oscillation frequency). A modified energy-based definition of the galloping instability parameter is used to compare the galloping instability of the oscillating cylinders to that based on quasi-steady behavior. The results show that the oscillating cylinders exhibit an instability parameter that is higher than that based on quasi-steady behavior, becoming increasingly so with the decrease in Reynolds number and reduced velocity. The latter monotonic trend with U_r is valid provided that shear layer reattachment does not occur during the oscillation. If reattachment occurs, it appears to lead to decreased susceptibility to galloping with decreasing U_r. The latter conclusion is based on limited observations and additional future work is needed for confirmation.

Significantly, it is found that the motion of the cylinder at low Reynolds number and reduced velocity causes shear layer reattachment on the surface at an effective angle of attack significantly lower than the geometrical angle of attack required for reattachment to occur on the bottom surface of a static cylinder. On the flip side, the excursion of the shear layer away from the cylinder surface during the oscillation is larger than that observed on the top surface of a static cylinder when the effective and static angles of attack are equal. These results demonstrate an unambiguous non-quasi-steady behavior of the separating shear layer, which is connected to the non-quasi-steady galloping force behavior. It is significant to note that this non-quasi-steady behavior is different from that traditionally involving the proximity of galloping and vortex shedding frequencies. The non-quasi-steady behavior identified here relates to the unsteady response of the boundary layer and the separated shear layer, rather than vortex shedding. This response is found to have a negligible effect on galloping instability when $U_r Re_d$ is approximately larger than 10^6. Thus, for Reynolds numbers well above those relevant to PADS suspension lines, the non-quasi-steady effects discovered in this study are likely not significant. This might be the reason why the type of non-quasi-steady behavior reported here has not been identified previously. Another possible reason is the difficulty to characterize the thin boundary layer regions on a moving test model. In this project, such characterization is enabled by the unique ability of 1c-MTV to provide high-resolution data at *every pixel* in an image.

VI. Outlook

At the conclusion of this project we have accumulated significant amount of force and velocity data on the static and oscillating cylinders. We plan to finish the main analyses of these data sets and publish the results in conference and journal papers. We have one SciTech 2022 abstract under review that is focused on static and dynamic analysis of 1c-MTV measurements in the wake of cylinders with and without surface topology. We also plan to prepare an expanded version of the results and discussion presented in §*VI* in a manuscript to be sent for archival journal publication in the near future.

VII. References

[1] Siefers, T., Greene, K., McLaughlin, T. and Bergeron, K. [2013] "Wind and water tunnel measurements of parachute suspension line," *51st AIAA Aerospace Sciences Meeting*, AIAA 2013-0064

[2] Siefers, T. M. [2013] "Flow and vibration analysis of parachute suspension line," MS Thesis, University of Colorado, Colorado Springs, Colorado

[3] Blevins, R. D. [2001] "Flow-induced vibration", Krieger Publishing Company, Florida

[4] Feero, M. A., Naguib, A. M. and Koochesfahani, M. M. [2019] "Single-component force balance for the measurement of low-magnitude mean aerodynamic loads," *Measurement Science and Technology* 30, 115301 (12 pp), DOI: 10.1088/1361-6501/ab2dd6

[5] Feero, M. A., Naguib, A. M. and Manoochehr, M. M. [2019] "Geometry effects on the galloping instability of rectangular cylinders at low Reynolds numbers," *AIAA SciTech Forum*, AIAA paper number 2019-1340, 7-11 January San Diego, CA, DOI: 10.2514/6.2019-1340

[6] Feero, M. A., Naguib, A. M. and Koochesfahani, M. M. [2020] "Influence of geometry on the galloping instability of rectangular cylinders in the Reynolds number range 1,000-10,000," *Journal of Fluids and Structures* 94, 102881 (15 pp), DOI:10.1016/j.jfluidstructs.2020.102881

[7] Feero, M. A., Naguib, A. M. and Koochesfahani, M. M. [2019] "Surface topology effects on the transverse galloping behavior of rectangular cylinders," *11th International Symposium on Turbulence and Shear Flow Phenomena (TSFP 11)*, July 30 – August 2, Southampton, UK

[8] Feero, M. A., Naguib, A. M. and Koochesfahani, M. M. [2020] "Effect of surface topology on the galloping instability of rectangular cylinders," *International Journal of Heat and Fluid Flow* 86, 108721 (10 pp), DOI: 10.1016/j.ijheatfluidflow.2020.108721

[9] Kalan, K., Feero, M. A., Naguib, A. M. and Koochesfahani, M. M. [2020] "Influence of surface topology on boundary layer and near-wake behavior of rectangular cylinders," *AIAA SciTech Forum 2020*, AIAA 2020-2034, 6-10 January 2020, Orlando, FA, DOI: 10.2514/6.2020-2034

[10] Kalan, K., Safaripour, A., Naguib, A. M. and Koochesfahani, M. M. [2021] "Characterization of the aerodynamics of rectangular cylinders with surface topology," *AIAA SciTech Forum 2021*, AIAA 2021-1322, 11-15 & 19-21 January 2021, Virtual Event, DOI: 10.2514/6.2021-1322

[11] Naudascher, E. and Rockwell, D. [1994] "Flow-induced vibrations – an engineering guide", CRC Press, New York